

Variations of the Great Plains Precipitation and Its Relationship with Tropical Central-Eastern Pacific SST

SONG YANG^{1*}, X. DING², AND D. ZHENG³

¹*NOAA's Climate Prediction Center, Camp Springs, Maryland*

²*Department of Land Surveying and Geo-Informatics, Hong Kong Polytechnic University, Hong Kong, China*

³*Center for Astrogeodynamics Research, Shanghai Astronomical Observatory, Chinese Academy of Sciences, 80 Nandan Road, Shanghai 20030, China*

*Corresponding author address: Dr. Song Yang, NOAA's Climate Prediction Center, 5200 Auth Road, Room 605, Camp Springs, MD 20746. E-mail: Song.Yang@noaa.gov

ABSTRACT

In this study, the authors investigate the time-frequency characteristics of the variations of Great Plains (GP) precipitation and its relationship with tropical central-eastern Pacific sea surface temperature (SST) by applying several advanced analyses. They focus on the dominant timescales of GP precipitation variations, the combined effects of multi-scale oscillating signals on the intensity of precipitation, and the variations of SST-precipitation relationships in time and frequency domains.

The variability of GP precipitation is characterized by strong annual and semi-annual signals (especially the former), which possess the most stable oscillating frequencies and the largest amplitudes. However, non-seasonal oscillation signals, which have smaller amplitudes and more variable oscillating frequencies with time, also contribute significantly to the variability of GP precipitation. The presence of these multi-scale oscillating signals is often evident during periods of heavy precipitation. On the other hand, the non-seasonal oscillating signals and annual and semi-annual signals are of opposite phase during the periods of deficient GP precipitation.

Strong correlations exist between the GP precipitation and the NINO3.4 (5°S-5°N, 170°W-90°W) SST, especially in the summertime. The strongest correlations appear near the zero-lag (simultaneous correlation) and reach a maximum when the SST leads the precipitation by one month. The GP precipitation increases (decreases) during El Niño (La Niña) episodes. The precipitation and SST are strongly related in the quasi-biennial, interannual, and interdecadal frequency bands, although their coherence is unstable and varies with time. In particular, significant relationships are found on semi-annual and annual timescales in the 1950s and on interannual timescales in the 1910s, 1940s, and 1980s. A particularly significant relationship appears on the biennial timescale in the 1980s.

1. Introduction

The U.S. Great Plains (GP), a major region of wheat and other crop growth, is located in a transitional zone between the relatively dry climate to the west and the wetter climate to the east. Here, the amount of water supply, which determines the growth of wheat crops, depends critically on the amount of precipitation. Thus, an improvement in understanding and predicting the variability of GP precipitation is of great scientific and socio-economic importance.

The GP precipitation varies significantly on different timescales. The variability of the precipitation is associated with many weather and climate extremes in the region such as summer heat waves (Klein 1952; Karl and Quayle 1981; Namias 1982; Chang and Wallace 1987; Lyon and Dole 1995) and winter blizzards accompanied by strong winds and blowing snow (see Schwartz and Schmidlin 2002). This precipitation variability is more commonly known for its

linkage to the drought and flood events in spring and summer seasons (Dickson 1980; Livezey 1980; Diaz 1983; Namias 1983, 1991; Trenberth et al. 1988; Palmer and Brankovic 1989; Mo et al. 1991; Trenberth and Branstator 1992; Bell and Janowiak 1995; Mo et al. 1995; Trenberth and Guillemot 1996; Mo et al. 1997). In particular, the recent 1988 drought and 1993 flood have aroused considerable public and scientific interests because of their severity and extent.

Although the variability of GP precipitation may be attributed largely by the internal dynamics of the atmosphere, it is also associated with the changes in boundary surface conditions such as the variations of sea surface temperature (SST), snow and ice cover, and soil moisture content (Namias 1983, 1991). A number of previous studies (Ropelewski and Halpert 1986; Trenberth et al. 1988; Palmer and Brankovic 1989; Bunkers and Miller 1996; Trenberth and Guillemot 1996; Montroy et al. 1998; Mauget and Upchurch 1999; Barlow et al. 2001; Castro et al. 2001; Englehart and Douglas 2002; Mauget 2003) have recognized the importance of the tropical central-eastern Pacific SST, which is commonly used to measure the conditions of El Niño/Southern Oscillation (ENSO). Specifically, the wet (dry) years generally correspond to El Niño (La Niña) events (Castro et al. 2001; Mauget 2003). ENSO affects the precipitation through its influence on the jet stream and storm tracks over the Pacific and North America (e.g., Trenberth and Guillemot 1996).

According to Ting and Wang (1997), the most dominant mode of the singular value decomposition analysis of the Pacific SST and U.S. precipitation is characterized by an apparent feature linking the summertime precipitation of central U.S. to the influence of tropical Pacific SST. This result has also been supported by Lau and Weng (2002) and Lau et al. (2004a, b). Lau et al. (2002) further demonstrate a linkage between the tropical Pacific SST and the predictability of central-U.S. summer precipitation. Furthermore, the preliminary analysis by Li et al. (2004) indicates that, among the 12 U.S. domains classified by the National Oceanic and Atmospheric Administration (NOAA; see Fig. E5 in Climate Diagnostics Bulletin, November 2003), the Great Plains is the only region whose annual precipitation and the precipitation averaged for every season are significantly related to ENSO.

In their studies that focus on the North American monsoon, Higgins and Mo (1998) and Higgins and Shi (2000) clearly relate the variability of monsoon precipitation and Southwest precipitation to the season-to-season memory of the coupled ocean-atmosphere system over the tropical eastern Pacific. The result implies an impact of ENSO on the GP precipitation, which changes oppositely to the Southwest precipitation and is controlled by the North American monsoon anticyclone over western U.S. (see also Higgins et al. 1997). The variability of Southwest Plains precipitation has also been linked to the memory effect of spring snowpack over the southern Rocky Mountains, which may also be related to the anomalies of Pacific SST (Gutzler 2000). Furthermore, strong relationships have been found between ENSO and the precipitation over the larger-scale central United States (e.g. Hu and Feng 2001). In addition, the experiments with general circulation modes by Mo et al. (1991) and Atlas et al. (1993) also show the influence of tropical Pacific SST on GP precipitation, although the SST is not the only impacting factor.

In this study, we investigate further the variations of GP precipitation and its relationship with the ENSO-related SST of tropical central-eastern Pacific with the following objectives. We focus on the detailed features associated with the variations of precipitation and SST and address several aspects of these variations that have not been examined previously. We reveal the time-frequency characteristics of the variability of GP precipitation with an emphasis on the dominant timescales, and assess the contributions of dominant oscillating signals to the intensity of precipitation. Furthermore, we explore the SST-precipitation relationship in time and frequency domains. The study also emphasizes the importance of several advanced analysis tools, some of which have not been used previously to understand the variations of GP precipitation and its relations to ENSO-related SST.

In the next section, we describe the main features of the observational data and introduce the analysis methods applied in this study. The variability of GP precipitation in both time and frequency domains is investigated in Section 3. We present the details of the relationship between GP precipitation and tropical central-eastern Pacific SST in Section 4. Finally, we summarize the results in Section 5.

2. Data and Methods

a. Data

The data fields analyzed in this study are precipitation and SST. The precipitation is from the CRU TS 2.0 product (Mitchell et al. 2004) of the Climatic Research Unit (CRU) of the University of East Anglia in the United Kingdom. The dataset contains land-only data information for the period of 1901-2000, in a resolution of 0.5 degree (longitude) by 0.5 degree (latitude). It is a revision to the old (New et al. 2000) 0.5-degree time series, but according to Mitchell et al., the previous dataset should not be mixed with the current new dataset. More about the details of the CRU dataset can be found at the Web site <http://www.cru.uea.ac.uk/~timm>.

The SST comes from the NOAA Extended Reconstructed Sea Surface Temperature (ERSST; Smith and Reynolds 2003) dataset. The ERSST was constructed and updated by applying the most recently available SST in the Comprehensive Ocean-Atmosphere Data Set and using improved statistical methods that allow stable reconstruction with sparse data. It covers the time period from January 1854, in a grid of 2° (longitude) by 2°(latitude).

The popular NOAA reconstructed SST dataset has been used to force atmospheric general circulation models (e.g., Yang and Lau 1998; Gates et al. 1999), to assess model performance (Penland and Matrosova 1998), and to understand the coupled ocean-atmosphere processes (Zhang et al. 1997; Kinter et al. 2002), among others. The CRU dataset has also been applied widely in climate study for various purposes (e.g., George and Saunders 2001; Mariotti et al. 2002; Yang et al. 2002; Chen et al. 2003; Seth and Rojas 2003; Tippett et al. 2003). An important feature of these datasets is their long data records, which are necessary for the analyses carried out in the current work. According to Chen et al. (2003), there is an agreement between the CRU precipitation and the global land precipitation analysis based on gauge observations for the recent years since 1948 (see their Figs. 6 and 7). The GP precipitation analyzed here is the area-averaged data over the domain of 96°-105°W, 32°-49°N. As in Li et al. (2004), this Great Plains domain is adopted from the NOAA Climate Diagnostics Bulletin (e.g., November 2003; Fig. E5). It has been used for climate diagnostics and prediction purposes for many years. The tropical central-eastern Pacific SST is represented by the NINO3.4 SST (area-averaged information over 5°S-5°N, 170°W-90°W; Barnston et al. 1997), which has often been used for measuring the conditions of ENSO. As in many climate datasets, the quality of data in the earlier years may not be as high as that in the recent time. However, it is always possible that the data of some regions is more reliable than that of other regions, even in the earlier years. Furthermore, compared to the data information of a specific grid-point, the values of area average are usually more superior in increasing data stability and reducing data errors.

b. Methods of analysis

We apply several advanced tools to understand the features about the variability of GP precipitation and its relationship with NINO3.4 SST. Some aspects of these features have never been examined previously. We first apply the techniques of wavelet analysis and least-squares method to depict the time-frequency features and the dominant oscillating timescales of GP precipitation. We then use a multi-stage filter and a leap-step time series analysis model to understand the combined effects of multi-scale oscillating signals on precipitation variations. More about the methods for these analyses is discussed in Section 3.

For the relationship between GP precipitation and tropical central-eastern Pacific SST, we analyze the features of lead-lag correlation and their seasonality. In particular, we focus on the variability of the SST-precipitation relationship in both time and frequency domains, which has not been documented previously, by applying a technique in which a multiple moving-window method is used (see Section 4 for details).

3. Variability of Great Plains Precipitation

In this section, we depict the variability of GP precipitation with an emphasis on the time-frequency characteristics. We illustrate the wave spectra of the precipitation and explore the impact of multi-scale oscillating signals on the intensity of precipitation.

To facilitate the following discussion of this paper, we first show in Fig. 1 the monthly and seasonal variations of GP precipitation. The upper panel, presenting the monthly precipitation anomalies in which the mean annual cycle has been removed, indicates that the monthly fluctuation of GP precipitation has the same magnitude of the total precipitation, which maximizes in June (see the monthly climatology shown in the second panel). Values of seasonal mean precipitation (lower 4 panels) are highest in June-July-August (JJA), followed by March-April-May (MAM), and lowest in December-January-February (DJF). Note that precipitation variability on interannual and longer timescales exists for all seasons. In particular, the JJA values are extremely high in 1993 and 1915, and low in 1936 and 1934. The JJA precipitation deficit in the 1930s can also be seen in MAM and SON (September-October-November).

To improve our understanding of the variability of GP precipitation, we perform more detailed analyses. First, we apply time-frequency wavelet transform and related analyses to reveal the time-frequency characteristics of the precipitation variations. Wavelet analysis has been applied to address different issues of the Earth sciences including meteorology (e.g., Morlet et al. 1982; Chao and Naito 1995; Lau and Weng 1995; Torrence and Compo 1998; Zheng et al. 2000; Ding et al. 2002). In this study, we employ the method of Morlet et al. (1982). For a time series $f(t)$, its wavelet transform is defined as:

$$W_{\psi}(f)(a,b) = \frac{1}{\sqrt{a}} \int_{-\infty}^{\infty} f(t) \psi\left(\frac{t-b}{a}\right) dt \quad (1)$$

where $\psi(t)$ is the basic wavelet; a is the dilation/compression scale factor defining the characteristic frequency; and b is the translational factor in the time domain. As seen from Eq. (1), one of the advantages of the wavelet transform is that it can describe the spectra characteristics of time series $f(t)$ in the time-frequency domain (or a - b space).

In our computations, we first remove the known dominant annual cycle from the monthly precipitation series to better describe the characteristics of other frequencies. The estimated time-frequency spectra from the wavelet transform for the anomaly series without the mean annual signal (see Fig. 1; top panel) are shown in Fig. 2. It should be pointed out that removal of the annual cycle from the original data is not necessary because the wavelet analysis separates the signals for various frequencies. However, our comparison indicates that the features of other frequencies can be eye-captured more easily from Fig. 2, given the known feature that the annual cycle is the most dominant and stable signal as shown in Table 1 (also Figs. 3-4) later.

Strong signals appear from Fig. 2 on interannual timescales, especially on 2-4 years, indicating that the GP precipitation fluctuates on the timescales of biennial oscillation and ENSO phenomena, among others. Figure 2 also shows that the precipitation varies on interdecadal timescales (about 10 and 20 years); however, the variations are relatively weaker. In addition, the figure shows irregular higher-frequency spectral signals on intraseasonal timescales, although monthly data are unable to depict the intraseasonal features in the high-frequency (e.g. 20-30 days) band.

We further determine the magnitudes and phases of the temporal variations of GP precipitation by applying the method of least squares, which enables an identification or

estimation of stable parameters. We focus on the features of annual, semi-annual, interannual, and interdecadal timescales as well as the constant and linear trend terms. For this purpose, we use the original series of monthly precipitation including the seasonal signals. The least-squares method of Householder transform (see Powell and Reid 1969; Feng et al. 1978), which is a linear regression problem, is given as follows:

$$SL_t = a + bt + \sum_{k=1}^7 c_k \sin(2\pi t / P_k + \varphi_k) + \varepsilon_t \quad (2)$$

where P_k , c_k , and φ_k are, respectively, the periods, amplitudes, and phases of the annual, semi-annual, interannual, and interdecadal terms; and a and b are the constant and linear terms. Three interannual and two interdecadal terms are included in the solution as detailed in the next paragraph. Since the periods of interannual and interdecadal fluctuations are relatively unstable (see Fig. 2), we determine their mean values by the method of trial and error in the process of least-squares computations.

Shown in Table 1 is the information estimated for seven terms (annual, semi-annual, three interannual, and two interdecadal) in Eq. (2) for the monthly GP precipitation. The selection for the number of modes is based on the wavelet spectra estimated from Fig. 2 and the periods are identified by the means of least squares adjustment of Householder transform. The phase estimation is referenced to the epoch of January 1901. (When estimating the parameters of periodic signals, the beginning, middle, or end epoch of the data series are usually taken as the reference epoch.) It can be seen that the annual and semi-annual variations (rows 8 and 9) have the largest amplitudes (31.85 and 5.66 mm per month, respectively) and the most stable estimates of phases (see the values of root-mean-squares (RMS) of ± 1.1 and ± 6.3 in the last column). The analysis also identifies apparent fluctuations on interannual (rows 5-7) and interdecadal timescales (rows 3-4). In particular, the estimated timescales of 19.68 and 11.17 years are consistent with the interdecadal timescales of 20 and 12 years found by Hu et al. (1998) for the variability of annual precipitation over the central U.S. The estimated values of amplitudes for these fluctuations can reach about 2 mm per month and more. However, the phases of these fluctuations are unstable with larger standard deviations. Table 1 also indicates that there exists an increasing tendency in the GP precipitation, with a mean rate of 0.47 mm/month per decade during the last century. If this tendency is maintained, the GP precipitation at the end of this century will be 4.7 mm per month larger than at present.

The RMS value of ± 15.26 mm per month shown in Table 1 is calculated from the residual series after the seven oscillation signals (rows 3-9) and the constant and linear trend terms given in the table have been removed from the monthly precipitation data. The contribution of the frequency-oscillating signals detected by the wavelet spectrum to the RMS of monthly precipitation (± 27.65 mm per month) is about 45%, calculated as $(27.65 - 15.26) / 27.65$. It is known from the estimates of amplitude and standard deviation for the phases (see Table 1) that annual and semi-annual timescales, especially former, have the strongest oscillating signals with the most stable oscillating frequency. Therefore, most of the above-mentioned contribution should come from the seasonal oscillations.

The above analysis has quantitatively demonstrated the mean dominant oscillating signals of the variability of GP precipitation. Here, we study the combined effects of these multi-scale oscillating signals on precipitation variability. We first apply the technique of wavelet time-frequency spectra again, but to the original series of monthly precipitation (shown in Fig. 3, the upper panel for 1901-1950 and the third panel for 1951-2000), instead of the anomaly series. In Fig. 3, the frequency bands from intraseasonal to interannual timescales are displayed. By comparing the spectral signals in the various frequency bands to the monthly precipitation of the same time epochs, we are able to reveal the relationship between precipitation variations and the multi-timescale oscillating signals in the precipitation data. The dotted lines in Fig. 3 mark four

heavy precipitation periods: June 1915, June 1941, May 1957, and May 1982. It is found that spectral signals of increased precipitation (“warm” yellow and red colors), ranging from intraseasonal, annual, and quasi-biennial to interannual frequency bands, occur synchronously in these heavy precipitation epochs (also see Table 2 later). In contrast, for the four deficient precipitation periods in June 1910, June 1952, June 1980, and June 1988, “cool” color (green and blue) spectral signals appear on intraseasonal, quasi-biennial, and interannual timescales. (Here, warm color spectral signals also appear on the seasonal timescale in these summers, relative to other seasons, because of the nature of the annual cycle of GP precipitation.) Thus, the results from wavelet spectral analysis shown in Fig. 3 indicate, preliminarily, that the variations of GP precipitation are influenced strongly by the non-seasonal, multi-scale oscillation signals, in spite of the dominance of annual and semi-annual cycles.

We then extend our analysis of assessing the combined effects of multi-scale oscillations on GP precipitation variability by applying the Multi-Stage Filter (MSF) method that provides higher resolutions in the truncated frequency bands (Zheng and Dong 1986; Zheng and Luo 1992). The theoretical formula for the frequency response function R of the MSF is,

$$R = c(1 - A(f, e)^L)^M \quad (3)$$

In Eq. (3), c is a real constant, taken as 1 generally; L and M are positive integers, determined by the band-width of truncated frequencies; and $A(f, e)$ is the frequency response in the Vondrak’s smoothing method (Vondrak 1977):

$$A(f, e) = (1 + e^{-1} (2\pi f)^6)^{-1} \quad (4)$$

where f and e are, respectively, the corresponding frequency component and the smoothing factor.

The MSF method separates the signals of various timescales in the monthly precipitation data shown in Fig. 4a. Band passes of <0.3, 0.3-0.7, 0.7-1.3, 1.3-2.5, and 2.5-6.5 years (corresponding to intraseasonal, semi-annual, annual, quasi-biennial, and interannual timescales), are used respectively in the filtering process. Figure 4 shows the results obtained for the various timescales: intraseasonal (b), semi-annual (c), annual (d), quasi-biennial (e), and interannual (f). It should be noted that a so-called Leap-Step Time Series Analysis model (Zheng et al. 2000), which aims at improving the data information of end points in wavelet analysis, is also applied in the filtering process to reduce effectively the edge effects of the output signals.

Compared to Fig. 3, Fig. 4 demonstrates the combined effects of multi-scale oscillating signals on the variations of GP precipitation more quantitatively and more intuitively. It can be found from Fig. 4 that peak values occur almost synchronously for the four heavy precipitation periods in 1915, 1941, 1957, and 1982 on intraseasonal, quasi-biennial, and interannual timescales, besides the annual and semi-annual signals. For example, for the case of 1915, the peak values of annual and semi-annual signals are 36.4 and 1.8 mm per month, and those of intraseasonal, biennial, and interannual signals reach, respectively, to 7.2, 10.1, and 9.7 mm per month (see Table 2). For 1957, the peak values are 35.9 and 7.4 mm per month for the annual and semi-annual signals, and 14.3, 8.6, and 8.9 mm per month for the intraseasonal, quasi-biennial, and interannual timescales. During these two periods of heavy precipitation, the contributions by the interannual and quasi-biennial signals to the total precipitation is equivalent to 53% and 42% of those by the seasonal signals. Also, for both cases, the contribution of each non-seasonal signal is clearly larger than that of the semi-annual signal, differing from the mean feature shown in Table 1. On the other hand, during the four periods of deficient precipitation in 1910, 1952, 1980, and 1988 (lower portion of Table 2), lower peak values appear on the various time scales and opposite signs are apparent between the seasonal and non-seasonal signals. (The

peak values of the annual cycle are positive for both heavy and light precipitation conditions because of the generally heavier precipitation in summer than in other seasons.) These light precipitation events are often associated with heat waves, as recorded in 1952 (Klein 1952) and 1980 (Dickson et al. 1980; Livezey 1980; Karl and Quayle 1981; Namias 1982).

In the summer of 1993, major floods occurred in the central U.S. including part of the Great Plains domain analyzed in this study. Our analysis indicates that, for June 1993 whose monthly mean GP precipitation is 113.7 mm per month (anomaly of 29.9), the peak values of intraseasonal, semi-annual, annual, quasi-biennial, and interannual signals are 1.0, 12.3, 36.2, 9.0, and 0.5, respectively.

The above investigation indicates that both the wavelet analysis and the method of MSF consistently demonstrate the combined effects of multi-scale oscillating signals on the variations of GP precipitation. The results obtained may also possess a useful potential for precipitation prediction. Namely, heavy precipitation may be predicted for the summers when the peak values of ENSO (e.g., NINO3.4 SST; see next section) and quasi-biennial signals occur synchronously. On the other hand, when low values of ENSO and quasi-biennial signals occur, deficient precipitation may be foretold. The features discussed here are consistent with the results obtained by Joseph et al. (2000) who indicated that, in the Midwest U.S., extreme summer drought and flood events are manifestations of persistent anomalous dry or wet conditions across multiple timescales.

4. Relationship between Great Plains Precipitation and Tropical Pacific SST

One of the important features discussed in the above section is that the GP precipitation varies strongly on interannual timescale. Here, we carry out a further analysis to reveal the relationship between the precipitation and tropical Pacific SST including its time-frequency features and seasonal dependence. We particularly focus on the NINO3.4 SST, the data averaged over 5°S-5°N, 170°W-90°W.

Figure 5 shows the residual series of GP precipitation in which the seasonal signals and the constant and linear trend terms are removed (Fig. 5a) and its filtered series by a 6-month moving-average filter (Fig. 5b). A relationship is apparent between the filtered precipitation and the NINO3.4 SST shown in Fig. 5c. We first examine this relationship by analyzing the cross-correlation function in the time domain and the squared coherence spectrum in the frequency domain, between the two fields. Following Jenkins and Watts (1968), we compute the cross-correlation function $\rho(\tau)$ and squared coherence spectrum $\gamma^2(f)$ between the two time series as:

$$\rho(\tau) = \sigma_{12}(\tau) / (\sigma_{11}\sigma_{22})^{1/2} \quad (5)$$

$$R(f) = S_{12}(f) / (S_{11}(f)S_{22}(f))^{1/2} \quad (6)$$

$$\gamma^2(f) = |R(f)|^2 \quad (7)$$

In Eq. (5), σ_{12} is the cross-covariance function of phase lag τ ; and σ_{11} and σ_{22} are the variances of the two time series. In Eqs. (6) and (7), f is the frequency; $S_{12}(f)$ is the cross-power spectrum between the two time series; and $S_{11}(f)$ and $S_{22}(f)$ are the auto-power spectra of the two series, respectively. Here, the multi-window spectrum technique of Thomason (1982) is used in the calculations of power spectrum, with application of the Fourier transform.

Figure 6 shows the cross-correlation and cross-coherence, calculated by Eqs. (5)-(7), between NINO3.4 SST (Fig. 5c) and GP precipitation (Fig. 5a). Note that the constant and linear trend terms have been removed from the above series to meet the principle of statistics for correlation and coherence calculations. As seen from Fig. 6a, significant positive correlations between the SST and the precipitation appear near the zero-lag (simultaneous correlation) and reach a maximum when the SST leads the precipitation by one month. The positive correlations

indicate an increase (a decrease) in GP precipitation under the influence of El Niño (La Niña). These correlations exceed significantly the threshold value at the confidence level $\alpha=0.95$ determined by the Monte Carlo test (Zhou and Zheng 1999). In fact, significant correlations occur over a wide range of time, from the 11-month lead to the 6-month lag by the SST. (In the figure, values of negative lags represent the correlations in which SST leads precipitation.) Because of these broad bands of significant correlations, it seems difficult to claim a firm cause-and-effect relationship between the SST and the precipitation. The positive SST-precipitation relationship has also found by previous studies (e.g., Castro et al. 2001; Mauget 2003). Furthermore, it is consistent with the result of Higgins et al. (1999) who found that the North American monsoon precipitation, which varies out of phase with GP precipitation, decreases (increases) during El Niño (La Niña) years.

It can be seen from Fig. 6b that the SST has strong coherence with the precipitation on multiple frequency bands: 0.08-0.12, 0.20-0.22, 0.80-0.81, 1.37-1.42, 1.76-1.77, 1.87-1.90, 2.21-2.25, and 2.37-2.38 cycles per year. The values of coherence estimates for these frequency bands, which correspond to intraseasonal-interdecadal timescales, exceed significantly the threshold value at the 95% confidence level (Chao 1988). The largest coherence spectral peaks occur on decadal and intraseasonal timescales, exceeding significantly the threshold value of 0.54 at the 99% confidence level.

It should be pointed out that the cross-coherence estimations discussed above only represent the mean features of the entire time span and the squared coherence information in the frequency domain. They are unable to depict the stability and variability of the features in specific frequency bands with respect to time process over the data span. As shown by Hu and Feng (2001), the intensity of the teleconnection of ENSO with precipitation over central U.S. varies on interdecadal timescales. Thus, we now explore the coherence features between NINO3.4 SST and GP precipitation in both time and frequency domains by applying a new technique in which a moving window is used. With this method, the coherence in time-frequency domains are derived first by estimating the values of a sub-series of ten years and then by moving successively the data points for subsequent estimations.

Figure 7a shows the time-frequency coherence between the SST and the precipitation in frequency bands up to 3 cycles per year. In the figure, the coherence intensities are presented by the various colors and the confidence levels of coherence estimates are shown by the dashed lines in the color bar on the right-hand side of the figure. The figure indicates that significant coherence estimates between NINO3.4 SST and GP precipitation appear mainly in the lower frequency bands up to one cycle per year, especially on interannual timescales. In addition, large coherence appears in the frequency bands of about 7-10 months in the 1920s-1930s and 5.5-7.5 in the 1950s. It can be seen from the figure that the coherence estimates are unstable and vary with time in all frequency bands. This manifests the advantage of this method in depicting the detailed features of the relationship between NINO3.4 SST and GP precipitation.

One of the important features shown in Fig. 7a is that the significance of the SST-precipitation relationship shifts among different frequency bands in different decades. To reveal this feature more clearly, we zoom in its specific aspects, respectively, for several time periods. It can be seen from Fig. 7b that significant SST-precipitation relationships occur on biennial and ENSO timescales (about 20-60 months) before the 1920s and in the early 1940s, and on semi-annual timescale (about 7-10 months) from the late 1920s to the early 1930s. The NINO3.4 SST coheres significantly with the GP precipitation on the timescales of about 13-24 months during 1948-54 and about 6-7.5 months (semi-annual) during 1950-60 (Fig. 7c). A particularly strong SST-precipitation relationship is found between 1982-88 on biennial timescale (see Fig. 7d). During this period, the NINO3.4 SST and the GP precipitation are also related strongly on ENSO timescale, about 30-60 months.

During the past decades, several major El Niño events have occurred in 1957/58, 1965/66, 1972/73, 1982/83, 1991/92, and 1997/98; and major La Niña events in 1955/56, 1973/74, 1975/76, 1988/89, and 1998/99 (see http://www.cpc.ncep.noaa.gov/products/analysis_monitoring/ensostuff/ensoyears.html). It may be interesting to note from Fig. 7 that, during these events, significant relationships between NINO3.4 SST and GP precipitation appear in different frequency bands (no information since the 1996 because of the truncation resulted from the data-filtering technique). For example, during the 1982/83 and 1988/89 episodes, the SST and the precipitation are mainly related on quasi-biennial and longer timescales. However, during the 1957/58 episode, they are coherent mainly on semi-annual timescale. The coherence between NINO3.4 SST and GP precipitation is generally weak in the 1970s. While the cause of this feature is a subject of future studies, the above results indicate that the SST-precipitation relationship is unstable with time and that the variability of GP precipitation does not respond linearly to the intensity of NINO3.4 SST. They also indicate the existence of other slowly-varying factors that affect the GP precipitation and its relationship with the tropical Pacific SST (see Ting and Wang 1997).

We now investigate the seasonality of the cross-correlation and cross-coherence between the seasonal GP precipitation (see Fig. 1) and NINO3.4 SST for MAM, JJA, SON, and DJF, respectively. Figure 8 shows the results for cross-correlation in (a) and those for cross-coherence in (b) calculated by Eqs. (5)-(7). The simultaneous correlations between the precipitation and the SST (Fig. 8a) exceed significantly the threshold value of 0.20 at the 95% confidence level determined by the Monte Carlo test (Zhou and Zheng 1999) in the seasons of spring, summer, and winter. Especially for summer, when the precipitation increases (decreases) in response to El Niño (La Niña), the correlation exceeds the threshold value of 0.26 at the 99% confidence level. In addition, the NINO3.4 SST leads (for MAM and JJA) and lags (for SON and DJF) the GP precipitation on decadal timescales. However, it is difficult to explain this feature without an understanding of the physics of any possible relationship between the SST and the precipitation on such long timescales, especially when the seasonality of the relationship is taken in account.

The bulk parts of the coherence spectral estimations (Fig. 8b) exceed significantly the threshold value of 0.39 at the 95% confidence level in multiple frequency bands for all seasons. For MAM, the frequency bands of significant coherence are 0.08-0.10 and 0.42-0.45 cycles per year (namely, on the timescales of about 10.0-12.5 and 2.2-2.4 years). For JJA, those significant bands are 0.10-0.12, 0.22, and 0.39-0.42 cycles per year (about 8.3-10.0, 4.5, and 2.4-2.6 years). The frequency bands of significant coherences occur in 0.12-0.18 cycles per year (5.6-8.3 years) for SON, and 0.12 and 0.19-0.20 cycles per year (8.3 and 5.0-5.3 years) for DJF. Strong coherence appears mainly in the low frequency band in SON and DJF, but higher frequencies in MAM and JJA. It can also be seen that the GP precipitation and the NINO3.4 SST are coherent on much longer timescales. A combination of the correlation and coherence features indicates that the precipitation and the SST have the strongest relationship on ENSO timescales in summer.

5. Summary and discussion

In this study, we have investigated the variations of U.S. Great Plains precipitation and its relationship with the tropical central-eastern Pacific SST by applying a number of advanced statistical tools. We have first used the techniques of wavelet analysis and least-squares method to depict the time-frequency features and the mean dominant oscillating timescales of the variability of GP precipitation. We have then used a multi-stage filter to demonstrate the combined effects of multi-scale oscillating signals on the variations of the precipitation. Furthermore, we have studied the lead-lag relationship between the precipitation and the tropical Pacific SST as well as the time-frequency features of their coherence, by employing a cross-covariance function analysis and a multiple moving-window method.

Among the timescales examined in this study (ranging from intraseasonal to interdecadal) for the variability of GP precipitation, annual and semi-annual signals, especially the former, have the most stable oscillating frequencies and the largest amplitudes. The non-seasonal oscillation signals have smaller amplitudes and more variable oscillating frequencies with time. However, the combined effects of multi-scale oscillating signals on the variations of precipitation are evident. The GP precipitation increases when the phases of the peaks of non-seasonal oscillating signals including intraseasonal, quasi-biennial, and interannual timescales are the same as those of seasonal signals. On the other hand, the precipitation decreases when the phases of non-seasonal oscillating signals are opposite to those of seasonal signals. During the periods of heavy precipitation, the contribution of interannual and quasi-biennial oscillating signals to the total precipitation can be equivalent to about 40-50% of that of the seasonal signals. The variability of GP precipitation should be related closely to the changes in both local and remote atmospheric circulation patterns. For example, the quasi-biennial signal of the precipitation may be linked to the variability of the Great Plains low-level jet.

The GP precipitation is significantly correlated with NINO3.4 SST and the strongest relationships appear near the zero-lag (simultaneous correlation) and reach a maximum when the SST leads the precipitation by one month. It increases (decreases) during El Niño (La Niña) episodes. Significant coherence between the precipitation and the SST occurs in quasi-biennial, interannual, and interdecadal frequency bands. An analysis of the time-frequency features of the coherence between the precipitation and the SST indicates that the coherence estimates are unstable and vary with time. Significant relationships are found on semi-annual timescale in the 1950s and on interannual timescales in the 1910s, 1940s, and 1980s. Particularly significant relationships appear on the biennial timescale in the 1980s and on the annual timescale from the late 1940s to the early 1950s. It is also found that the most significant correlation between the precipitation and the SST occurs in summertime, followed by winter and spring. However, even in SON, the GP precipitation is strongly related to NINO3.4 SST in the band of 5.5-8.5 years.

In brief, we have carried out this work with two main purposes: to conduct a pilot study of the applications of several advanced tools in precipitation analysis and to depict the time-frequency characteristics of the variations of GP precipitation and its relationship with tropical central-eastern Pacific SST. A number of interesting features have been revealed especially in the combined effects of multi-scale oscillating signals on GP precipitation and in the time-frequency characteristics of the relationship between the precipitation and NINO3.4 SST. However, to fully explain these features, substantial effort is needed to understand the associated changes in the dynamical processes of atmospheric, oceanic, and land surface conditions.

Acknowledgments. The authors thank Dr. Q. Li of the China Meteorological Administration for preparation of the precipitation and SST data. The comments from John Janowiak and Pingping Xie of NOAA's Climate Prediction Center are helpful for improving the quality of the paper. This study was jointly supported by the Hong Kong Research Grants Council (Project No. PolyU5067/00E), the Hong Kong Polytechnic University (Project No. G.34.37.YY42), the Natural Science Foundation of China and the Chinese Academy of Sciences (Projects 10133010, 10273018, and KJCX2-SW-T1), and the NOAA GEWEX Americas Prediction Project (GC03-322).

REFERENCES

- Atlas, R., N. Wolfson, and J. Terry, 1993: The effect of SST and soil moisture anomalies on GLA model simulations of the 1988 U.S. summer drought. *J. Climate*, **6**, 2034-2048.
- Barnston, A. G., M. Chelliah, and S. B. Goldenberg, 1997: Documentation of a highly ENSO-related SST region in the equatorial Pacific. *Atmosphere-Ocean*, **35**, 367-383.

- Bell, G. D., and J. E. Janowiak, 1995: Atmospheric circulation associated with the Midwest floods of 1993. *Bull. Amer. Meteor. Soc.*, **76**, 681-695.
- Burkers, M. J., and J. R. Miller, 1996: An examination of El Niño – La Niña-related precipitation and temperature anomalies across the northern Plains. *J. Climate*, **9**, 147-160.
- Castro, C. L., T. B. McKee, and R. A. Pielke, 2001: The relationship of the North American monsoon to tropical and North Pacific sea surface temperatures as revealed by observational analyses. *J. Climate*, **14**, 4449-4473.
- Chang, F.-C., and J. M. Wallace, 1987: Meteorological conditions during heat waves and droughts in the United States Great Plains. *Mon. Wea. Rev.*, **115**, 1253-1269.
- Chao, B. F., 1988: Correlation of interannual length-of-day variation with El Niño/southern oscillation. *J. Geophys. Res.*, **93**, 7709-7715.
- Chao, B. F., and I. Naito, 1995: Wavelet analysis provide a new tool for study Earth rotation. *EOS*, **76**, 161.
- Chen, M., P. Xie, J. E. Janowiak, and P. A. Arkin, 2003: Global land precipitation: A 50-yr monthly analysis based on gauge observations. *J. Hydrometeor.*, **3**, 249-266.
- Diaz, H. F., 1983: Drought in the United States – Some aspects of major dry and wet periods in the contiguous United States, 1895-1981. *J. Climatol. Appl. Meteor.*, **22**, 3-16.
- Dickson, R. R., 1980: Weather and circulation of June, 1980 – Inception of a heat wave and drought over the central and southern Great Plains. *Mon. Wea. Rev.*, **108**, 1469-1474.
- Ding, X. L., D. W. Zheng, and S. Yang, 2002: Variations of the surface temperature in Hong Kong during the last century, *Int. J. Climatol*, **22**, 715–730.
- Englehart, P. J., and A. V. Douglas, 2002: On some characteristic variations in warm season precipitation over the central United States (1910-2000). *J. Geophys. Res.*, **107**, No. 4286.
- Feng, K., J. Zhang, Y. Zhang, Z. Yang, and W. Chao, 1978: *The Numerical Calculation Method*, National Defense Industry Press, pp. 311.
- Gates, W. L., J. S. Boyle, C. Covey, C. G. Dease, and Coauthors, 1999: An overview of the results of the Atmospheric Model Intercomparison Project (AMIP I). *Bull. Amer. Meteor. Soc.*, **80**, 29-55.
- George, S. E., and M. A. Saunders, 2001: North Atlantic Oscillation impact on tropical North Atlantic winter atmospheric variability. *Geophys. Res. Lett.*, **28**, 1015-1018.
- Gutzler, D. S., 2000: Covariability of spring snowpack and summer rainfall across the southwest United States. *J. Climate*, **13**, 4018-4027.
- Higgins, R. W., Y. Yao, and X. Wang, 1997: Influence of the North American monsoon system on the U.S. summer monsoon regime. *J. Climate*, **10**, 2600-2622.
- Higgins, R. W., and K. C. Mo, 1998: Interannual variability of the U.S. summer precipitation regime with emphasis on the southwestern monsoon. *J. Climate*, **11**, 2582-2606.
- Higgins, R. W., Y. Chen, and A. V. Douglas, 1999: Interannual variability of the North American warm season precipitation regime. *J. Climate*, **12**, 653-680.
- Higgins, R. W., and W. Shi, 2000: Dominant factors responsible for interannual variability of the summer monsoon in the southwestern United States. *J. Climate*, **13**, 759-776.
- Hu, Q., and S. Feng, 2001: Variations of teleconnection of ENSO and interannual variation in summer rainfall in the central United States. *J. Climate*, **14**, 2469-2480.
- Hu, Q., C. M. Woodruff, and S. E. Mudrick, 1998: Interdecadal variations of annual precipitation in the central United States. *Bull. Amer. Meteor. Soc.*, **79**, 221-229.
- Jenkins, G., and D. Watts, 1968: *Spectrum Analysis and Its Applications*, Holden-Day, San Francisco, CA.
- Joseph, R., M. Ting, and P. Kumar, 2000: Multiple-scale spatio-temporal variability of precipitation over the coterminous United States. *J. Hydrometeor.*, **1**, 373-392.
- Karl, T. R., and R. G. Quayle, 1981: The 1980 summer heat wave and drought in historical perspective, *Mon. Wea. Rev.*, **109**, 2055-2073.

- Kinter III, J. L., K. Miyakoda, and S. Yang, 2002: Recent change in the connection from the Asian monsoon to ENSO. *J. Climate*, **15**, 1203-1215.
- Klein, W. H., 1952: Weather and circulation of July, 1952 – A month with drought. *Mon. Wea. Rev.*, **80**, 118-122.
- Lau, K.-M., and H. Weng, 1995: Climate signal detection using wavelet transform: How to make a time series sing. *Bull. Amer. Meteor. Soc.*, **76**, 2391-2406.
- Lau, K.-M., K.-M. Kim, and S. S. P. Shen, 2002: Potential predictability of seasonal precipitation over the United States from canonical ensemble correlation predictions. *Geophys. Res. Lett.*, **29**, No. 1097.
- Lau, K.-M., and H. Weng, 2002: Recurrent teleconnection patterns linking summertime precipitation variability over East Asia and North America. *J. Meteor. Soc. Japan*, **80**, 1309-1324.
- Lau, K.-M., K.-M. Kim, and J.-Y. Lee, 2004a: Interannual variability, global teleconnection, and potential predictability associated with the Asian summer monsoon. *East Asian Monsoon* (Eds. C.-P. Chang), World Scientific Publisher, in press.
- Lau, K.-M., J.-Y. Lee, K.-M. Kim, and I.-S. Kang, 2004b: The North Pacific as a regulator of summertime climate over Eurasia and North America, *J. Climate*, **17**, 819-833.
- Li, Q., S. Yang, R. W. Higgins, V. E. Kousky, K.-M. Lau, and P. Xie, 2004: Variations of U.S. and China precipitation: Regional manifestations of large-scale climate phenomena. *Meteor. Atmos. Phys.*, to be submitted.
- Livezey, R. E., 1980: Weather and circulation of July, 1980 – Climax of historical heat wave and drought over the United States. *Mon. Wea. Rev.*, **108**, 1708-1716.
- Lyon, B., and R. M. Dole, 1995: A diagnostic comparison of the 1980 and 1988 U.S. summer heat wave-droughts. *J. Climate*, **8**, 1658-1676.
- Mariotti, A., M. V. Struglia, N. Zeng, and K.-M. Lau, 2002: The hydrological cycle in the Mediterranean region and implications for the water budget of the Mediterranean Sea. *J. Climate*, **15**, 1674-1690.
- Marlow, M., S. Nigam, and E. H. Berbery, 2001: ENSO, Pacific decadal variability, and U.S. summertime precipitation, drought, and stream flow. *J. Climate*, **14**, 2105-2128.
- Mauget, S. A., 2003: Intra- to multidecadal climate variability over the continental United States: 1932-99. *J. Climate*, **16**, 2215-2231.
- Mauget, S. A., and D. R. Upchurch, 1999: El Niño and La Niña related climate and agricultural impacts over the Great Plains and Midwest. *J. Produc. Agricul.*, **12**, 203-215.
- Mitchell, T. D., T. R. Carter, P. D. Jones, M. Hulme, and M. New, 2004: A comprehensive set of high-resolution grids of monthly climate for Europe and the globe: the observed record (1901-2000) and 16 scenarios (2001-2100). *J. Climate*, submitted.
- Mo, K. C., J. R. Zimmerman, E. Kalnay, and M. Kanamitsu, 1991: A GCM study of the 1988 United States drought. *Mon. Wea. Rev.*, **119**, 1512-1532.
- Mo, K. C., J. Nogués-Paegle, and J. Paegle, 1995: Physical mechanisms of the 1993 summer floods. *J. Atmos. Sci.*, **52**, 879-895.
- Mo, K. C., J. Nogués-Paegle, and R. W. Higgins, 1997: Atmospheric processes associated with summer floods and droughts in the central United States. *J. Climate*, **10**, 3028-3046.
- Montroy, D. L., M. B. Richman, and P. J. Lamb, 1998: Observed nonlinearities of monthly teleconnections between tropical Pacific sea surface temperature anomalies and central and eastern North American precipitation. *J. Climate*, **11**, 1812-1835.
- Morlet, J., G. Arehs, I. Fourgeau, and D. Giard, 1982: Wave propagation and sampling theory. *Geophysics*, **47**, 203-221.
- Namias, J., 1982: Anatomy of Great Plains protracted heat waves (especially the United States summer drought). *Mon. Wea. Rev.*, **110**, 824-838.
- Namias, J., 1983: Some causes of United States drought. *J. Climate Appl. Meteor.*, **22**, 30-39.

- Namias, J., 1991: Spring and summer 1988 drought over the contiguous United States – Causes and prediction. *J. Climate*, **4**, 54-65.
- National Oceanic and Atmospheric Administration, 2003: *Climate Diagnostics Bulletin*. Ed. By NOAA's Climate Prediction Center, November 2003.
- New, M., M. Hulme, and P. Jones, 2000: Representing twentieth-century space-time climate variability. Part II: Development of 1901-96 monthly grids of terrestrial surface climate. *J. Climate*, **13**, 2217-2238.
- Palmer, T. N., and C. Brankovic, 1989: The 1988 United States drought linked to anomalous sea surface temperature. *Nature*, **338**, 54-57.
- Penland, C., and L. Matrosova, 1998: Prediction of tropical Atlantic sea surface temperatures using Linear Inverse Modeling. *J. Climate*, **11**, 483-496.
- Powell, M., and J. Reid, 1969: On applying Householder's method to linear least squares problem. In Proceedings IFIP Congress 1968 (A. Morell Ed.), North-Holland, Amsterdam, pp. 122-126.
- Ropelewski, C. F., and M. S. Halpert, 1986: North American precipitation and temperature patterns associated with the El Niño/Southern Oscillation (ENSO). *Mon. Wea. Rev.*, **114**, 2352-2362.
- Schwartz, R. M., and T. W. Schmidlin, 2002: Climatology of blizzards in the conterminous United States, 1959-2000. *J. Climate*, **15**, 1765-1772.
- Seth, A., and M. Rojas, 2003: Simulation and sensitivity in a nested modeling system for South America. Part I: Reanalyses boundary forcing. *J. Climate*, **16**, 2437-2453.
- Smith, T. M., and R. W. Reynolds, 2003: Extended reconstruction of global sea surface temperatures based on COADS data (1854-1997). *J. Climate*, **16**, 1495-1510.
- Thomason, D., 1982: Spectrum estimation and harmonic analysis. *IEEE Proc.*, **70**, 1055-1096.
- Ting, M., and H. Wang, 1997: Summertime U.S. precipitation variability and its relation to Pacific sea surface temperature. *J. Climate*, **10**, 1853-1873.
- Tippett, M. K., M. Barlow, and B. Lyon, 2003: Statistical correlation of central Southwest Asia winter precipitation simulations. *Int. J. Climatol.*, **23**, 1421-1433.
- Torrence, C., and G. P. Compo, 1998: A practical guide to wavelet analysis. *Bull. Amer. Meteor. Soc.*, **79**, 61-78.
- Trenberth, K. E., G. W. Branstator, and P. A. Arkin, 1988: Origins of the 1988 North American drought. *Science*, **242**, 1640-1645.
- Trenberth, K. E., and G. W. Branstator, 1992: Issues in establishing causes of the 1988 drought over North America. *J. Climate*, **5**, 159-172.
- Trenberth, K. E., and C. J. Guillemot, 1996: Physical processes involved in the 1988 drought and 1993 floods in North America. *J. Climate*, **9**, 1288-1298.
- Vondrak, J., 1977: Problem of smoothing observational data II. *Bull. Astron. Inst.*, **28**, 83-93.
- Wang, H., and M. Ting, 2000: Covariabilities of winter U.S. precipitation and Pacific sea surface temperatures. *J. Climate*, **15**, 3711-3719.
- Yang, S., and K.-M. Lau, 1998: Influences of SST and ground wetness anomalies on the Asian summer monsoon. *J. Climate*, **11**, 3230-3246.
- Yang, S., K.-M. Lau, and K.-M. Kim, 2002: Variations of the East Asian jet stream and Asian-Pacific-American winter climate anomalies. *J. Climate*, **15**, 306-325.
- Zhang Y, J. M. Wallace, and D. S. Battisti, 1997: ENSO-like interdecadal variability: 1900-93. *J. Climate*, **10**, 1004-1020.
- Zheng, D. W., and D. N. Dong, 1986: Realization of narrow band filtering of the polar motion data with Multi-Stage Filter. *Acta Astronomica Sinica*, **27**, 368-376.
- Zheng, D. W., and S. F. Luo, 1992: Contribution of time series analysis to data processing of astronomical observations of Earth rotation in China. *Statistica Sinica*, **2**, 605-618.

- Zheng, D. W., B. F. Chao, Y. H. Zhou, and N. H. Yu, 2000: Improvement of edge effect of the wavelet time-frequency spectrum: Application to the length of day series. *J. Geodesy*, **74**, 249-254.
- Zhou, Y. H., and D. W. Zheng, 1999: Monte Carlo simulation test of correlation significance levels. *Acta Geodaetica et Cartographica Sinica*, **22**, 313-318.

Table 1. Estimates of the amplitudes and phases of oscillation signals of GP precipitation, ranging from seasonal to interdecadal timescales, derived by the least-squares method of Householder transform. The estimated phases in the table are referenced to the epoch of January 1901.

Precipitation variations		
Period (in year)	Amplitude (in mm/month)	Phase (in degree)
19.68	2.03±0.63	10.6±17.5
11.17	1.90±0.62	-63.6±18.8
4.49	1.79±0.62	50.8±20.0
3.00	2.37±0.62	-129.7±15.0
2.00	2.27±0.62	-3.7±15.7
1.00	31.85±0.62	-75.4±1.1
0.50	5.66±0.62	-162.8±6.3
Linear trend: 0.47±0.015 mm/month/decade		
RMS: ±15.26 mm/month		

Table 2. Precipitation rates (mm per month) identified for different time scales. Results are shown for four heavy (upper portion) and four light (lower portion) precipitation events, respectively.

Heavy Precipitation Events				
	June 1915	June 1941	May 1957	May 1982
Intraseasonal	7.2	28.8	14.3	2.5
Semi-annual	1.8	-15.9	7.4	16.0
Annual	36.4	34.8	35.9	34.4
Quasi-biennial	10.1	3.9	8.6	0.8
Interannual	9.7	11.3	8.9	7.1
Monthly mean	121.4	125.0	131.9	137.6
(Anomaly)	(37.6)	(41.2)	(53.5)	(59.2)
Light Precipitation Events				
	June 1910	June 1952	June 1980	June 1988
Intraseasonal	-4.7	-9.0	-4.0	-6.5
Semi-annual	1.9	4.0	-6.6	-4.0
Annual	26.1	28.3	25.8	25.8
Quasi-biennial	-3.5	-10.8	-4.3	0.6
Interannual	-5.8	-1.6	-6.5	-7.2
Monthly mean	49.8	54.3	56.7	55.8
(Anomaly)	(-34.0)	(-29.5)	(-27.1)	(-28.0)

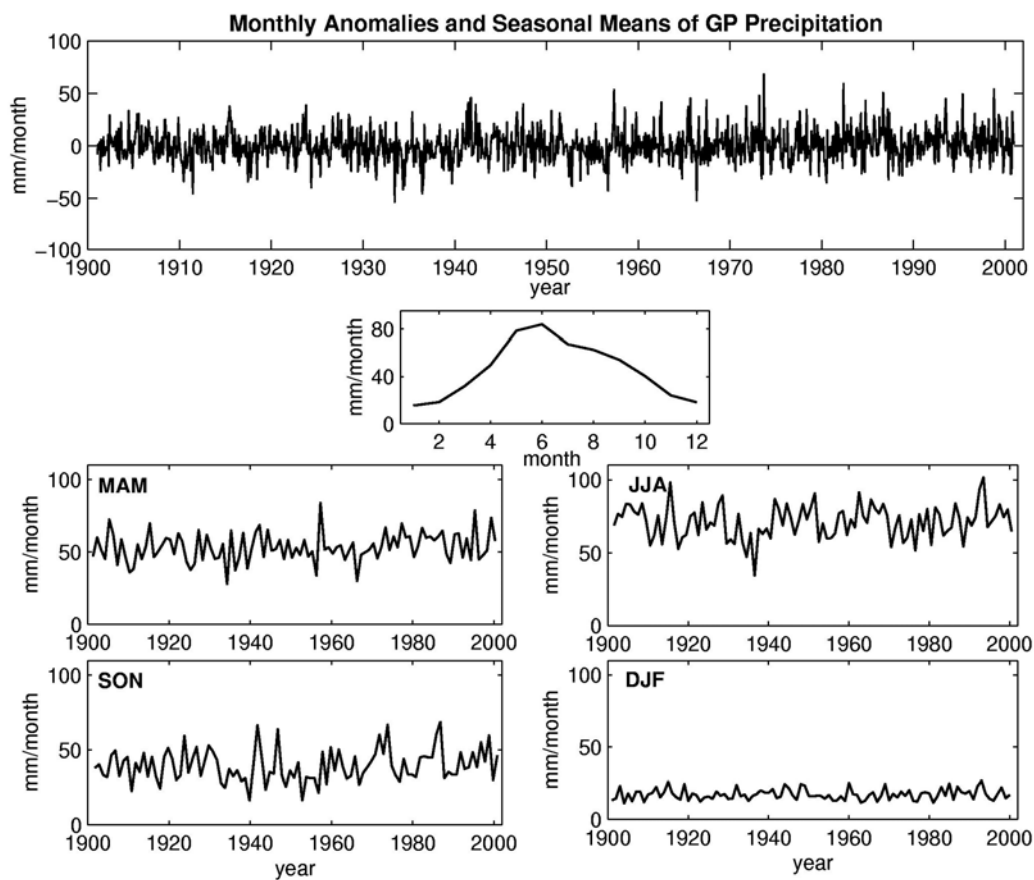


Fig. 1. Monthly anomalies in which the mean annual cycle is removed (top panel), mean annual cycle (second panel), and seasonal means (lower four panels) of the GP precipitation (mm per month). MAM, JJA, SON, and DJF stand for March-April-May, June-July-August, September-October-November, and December-January-February, respectively.

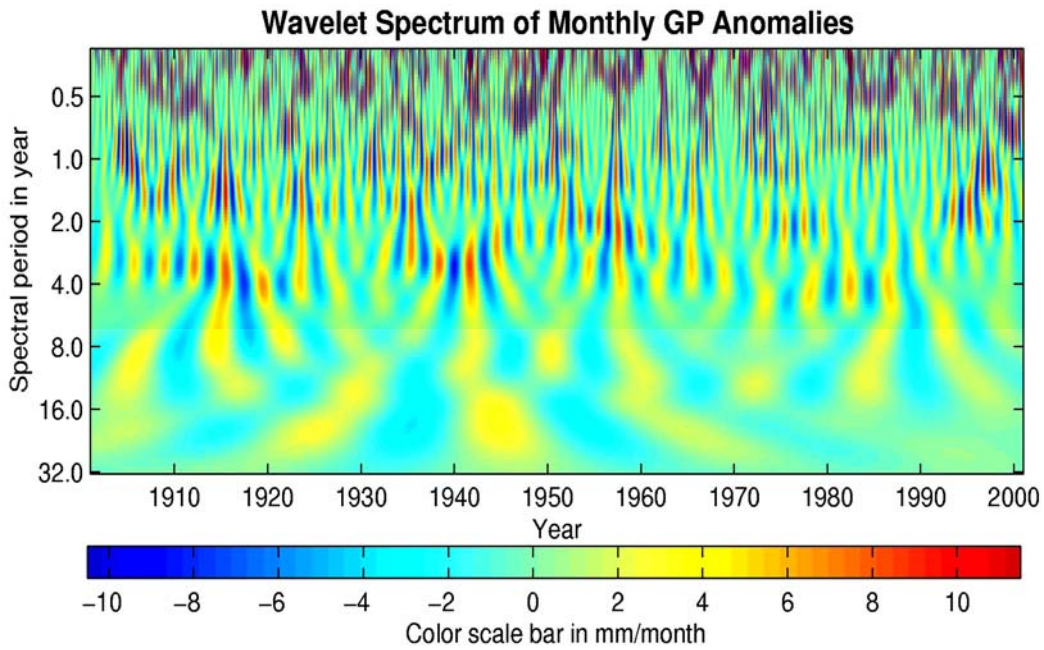


Fig. 2. Estimations of the time-frequency spectra of wavelet transform derived from the anomalous GP precipitation (see top panel in Figure 1). The red and blue colors represent the largest positive and negative amplitudes of wavelet spectra, respectively. The y-coordinate represents the periodic timescales of the time-frequency spectra.

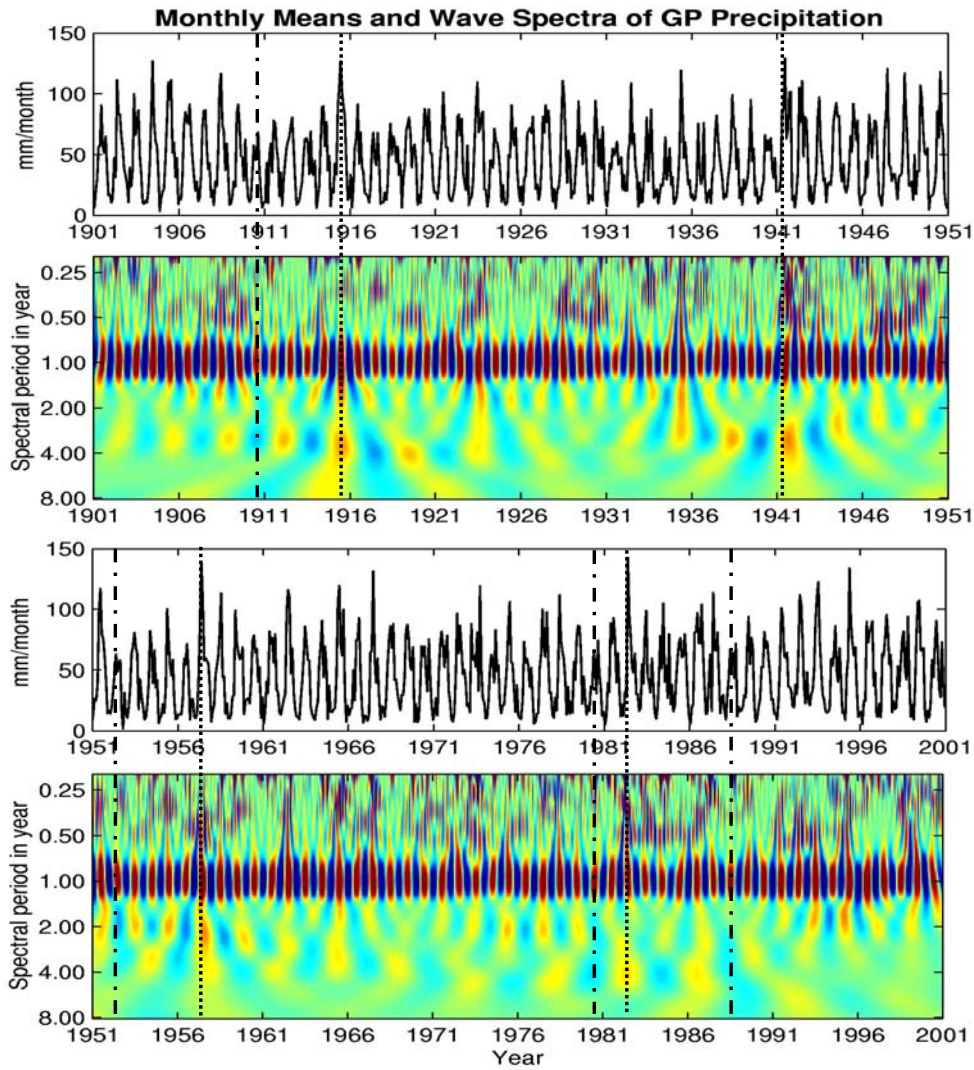


Fig. 3. Wavelet time-frequency spectra demonstrating the combined effects of multi-scale oscillating signals on the intensity of GP precipitation in the ranges of 0.2-8 years. The yellow and red colors indicate an increase in precipitation in the corresponding frequency bands, while green and blue indicate a decrease in precipitation. The curve shows the monthly precipitation. To increase the clarity of the figure, results for the entire time period are shown separately for two subsets of 1901-1950 and 1951-2000. The dotted (dashed) lines indicate four heavy (light) precipitation events (see text for details).

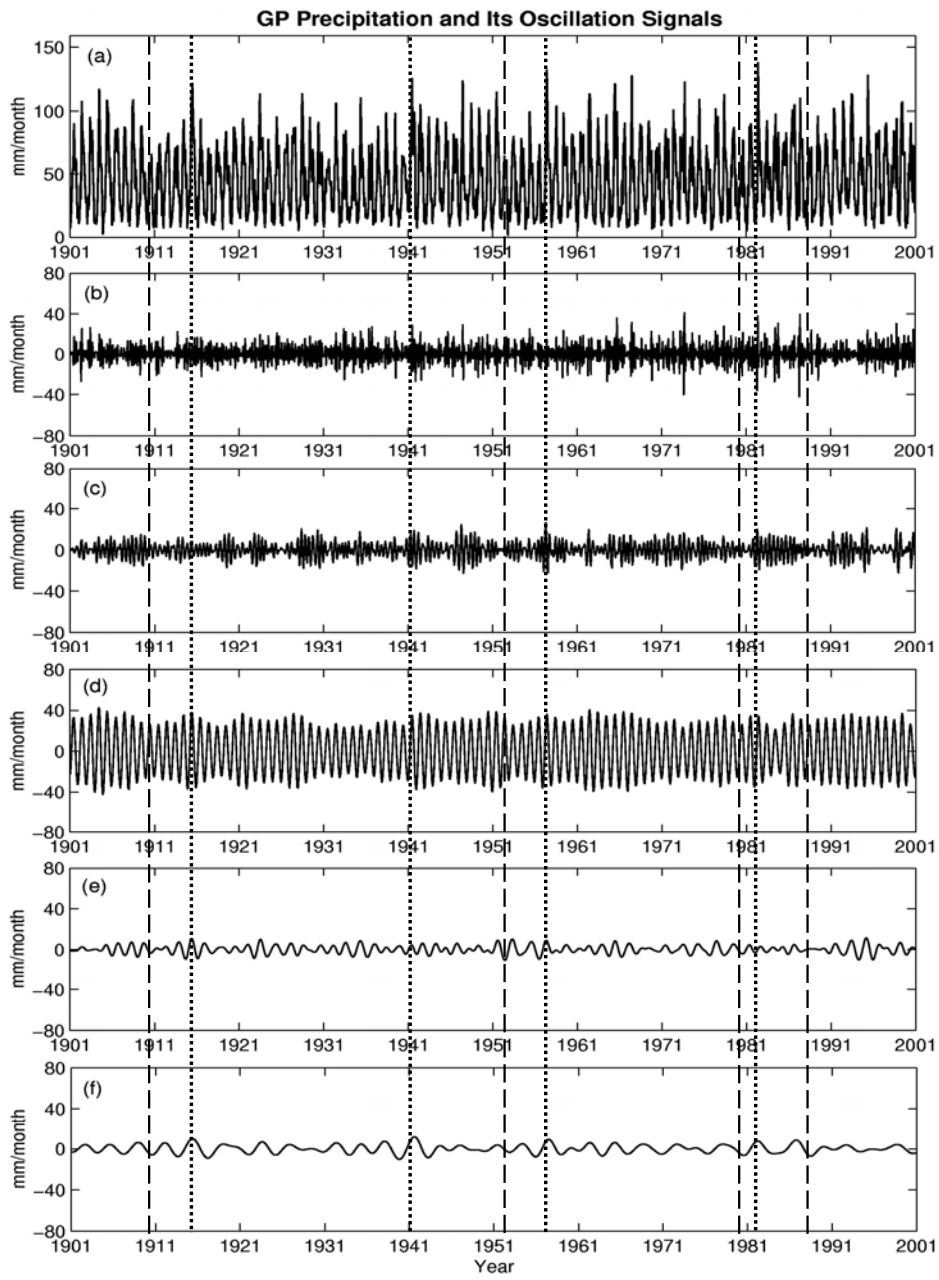


Fig. 4. Monthly GP precipitation (a) and oscillating signals on the intraseasonal (b), semi-annual (c), annual (d), quasi-biennial (e), and interannual (f) timescales. The dotted (dashed) lines indicate four heavy (light) precipitation events (see text for details).

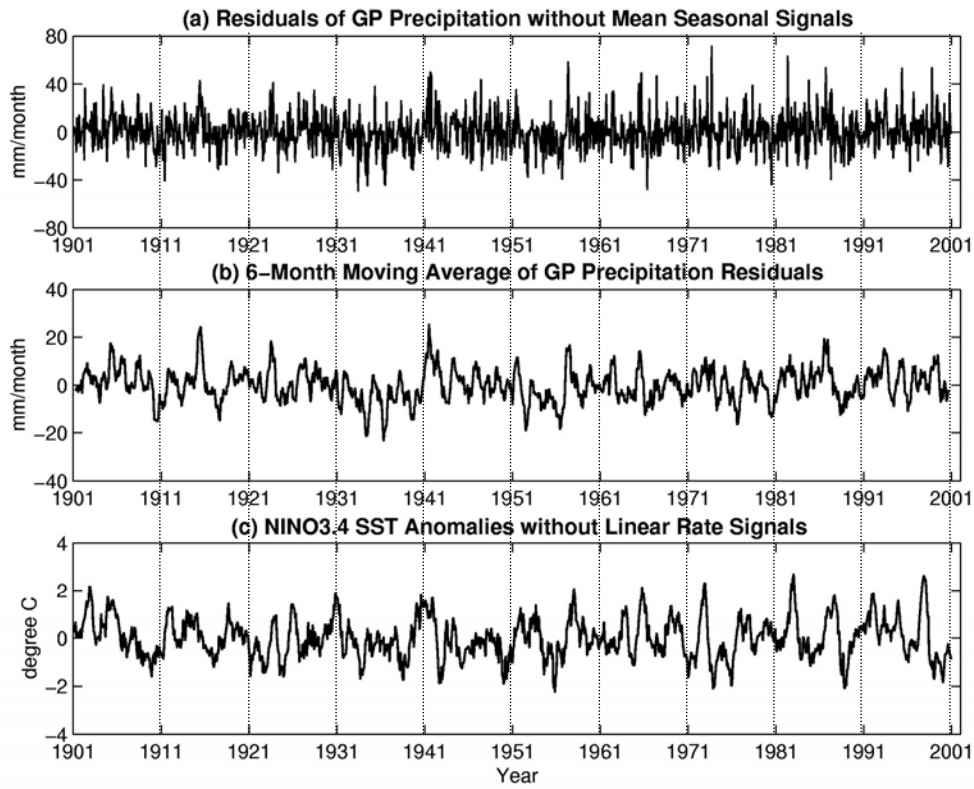
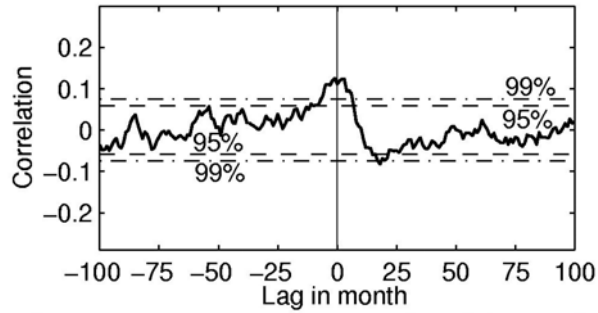


Fig. 5. (a) Residual series of GP precipitation in which the seasonal cycles and constant and linear trend terms have been removed. (b) Filtered residuals of precipitation by a 6-month moving- average filter. (c) NINO3.4 SST ($^{\circ}\text{C}$) with the constant and linear trend terms removed.

(a) Cross-Correlation between NINO3.4 SST and GP Precip



(b) Cross-coherence between NINO3.4 SST and GP Precip

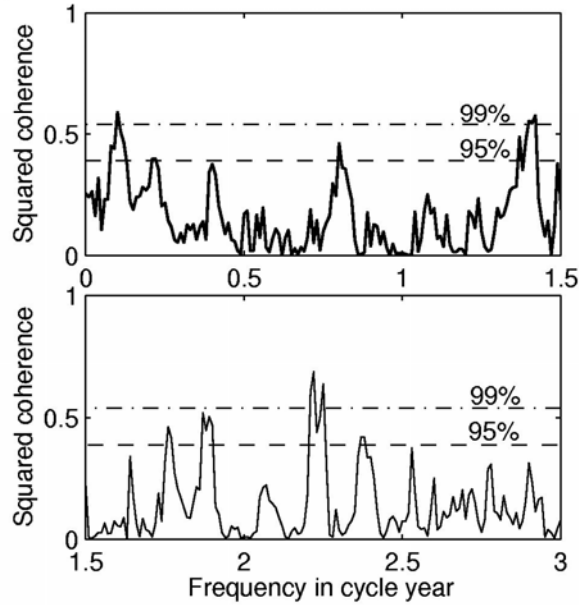


Fig. 6. Estimated cross-correlation (a) and squared coherence (b) between NINO3.4 SST and GP precipitation. Values of negative (positive) lags shown in the x-coordinate represent the correlations in which the SST leads (lags) the precipitation. The dashed lines show the threshold values of significant test (assessed two-sided) at the 95% and 99% confidence levels.

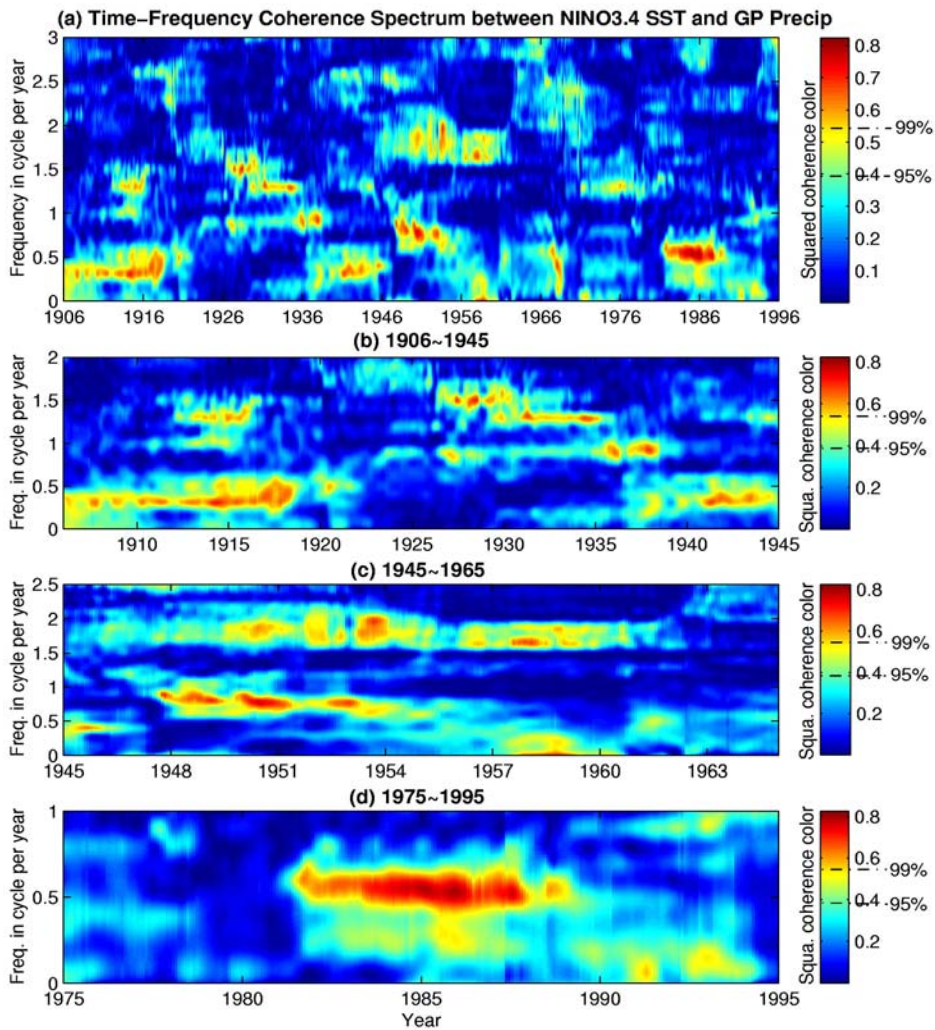


Fig. 7. (a) Estimations of coherence spectra between NINO3.4 SST (see Figure 5c) and GP precipitation (Figure 5a) shown in time-frequency domain. The threshold values of the significant test at the 95% and 99% confidence levels are given by the dashed-dotted lines in the color bar on the right-hand side of the figure. Note that a 5-year truncation occurs at each end of the figure. Shown also are the time-frequency features of the coherence spectra between NINO3.4 SST and GP precipitation zoomed in, respectively, for periods 1906-45 (Figure 7b), 1945-65 (7c), and 1975-95 (7d).

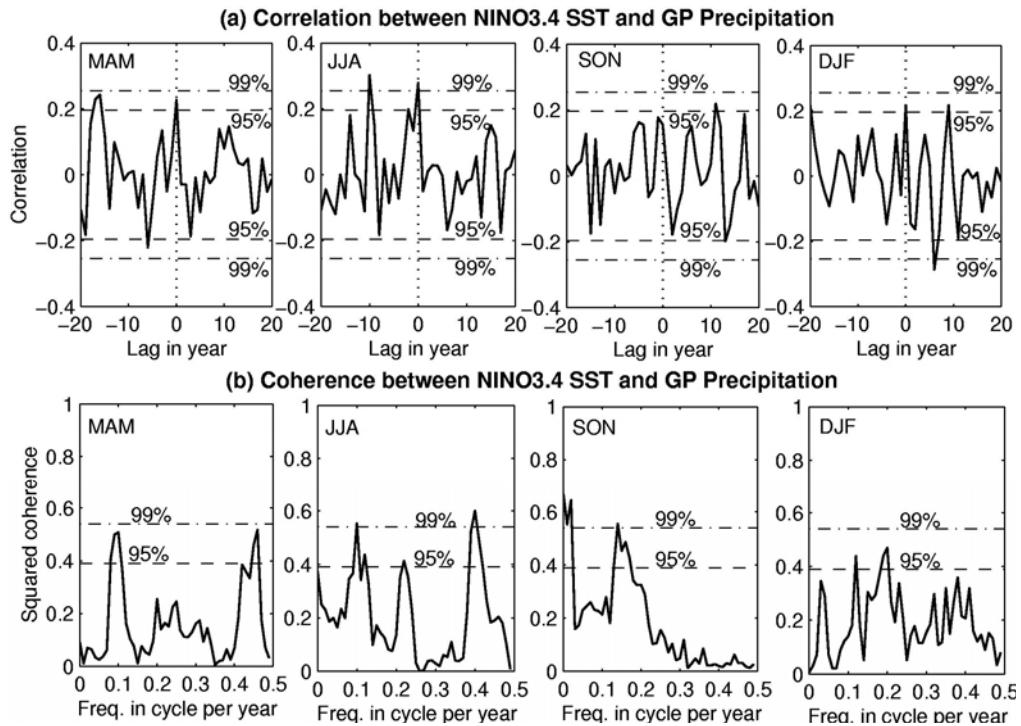


Fig. 8. Estimated cross-correlation (a) and squared coherence (b) between NINO3.4 SST and GP precipitation for the various seasons (MAM, JJA, SON, and DJF). Values of negative (positive) lags shown in the x-coordinate represent the correlations in which the SST leads (lags) the precipitation. The dashed lines show the threshold values of significant test at the 95% and 99% confidence levels.